



Generation and characteristics of hollow structured optical fields based on multiple off-axis vortices

YIPING GENG,¹ HAO HU,¹ XINRU MA,¹ XIAOXUE HU,¹ XINYUE CHAI,¹  XIAOLEI WANG,^{1,2,*} SIXING XI,^{3,6} AND ZHUQING ZHU^{4,5} 

¹Institute of Modern Optics, College of Electronic Information and Optical Engineering, Nankai University, Tianjin Key Laboratory of Micro-scale Optical Information Science and Technology, Tianjin 300350, China

²State Key Laboratory of Intense Pulsed Radiation Simulation and Effect, Xi'an 710024, China

³School of Mathematics and Physics, Hebei University of Engineering, Handan, Hebei 056038, China

⁴School of Computer and Electronic Information, Nanjing Normal University, Nanjing 210023, China

⁵State Key Laboratory of Applied Optics, Changchun Institute of Optics, Fine Mechanics and Physics, Chinese Academy of Sciences, Changchun 130033, China

⁶xisixing@126.com

*wangxiaolei@nankai.edu.cn

Abstract: In this paper, various hollow structured optical fields are generated by skillfully adjusting the number and positions of multiple off-axis vortices loaded in a Gaussian beam. The focal-field characteristics of the generated hollow structured optical fields after passing through an ordinary lens are studied based on the scalar diffraction theory. Firstly, a variety of hollow structured optical fields are theoretically simulated by adjusting the number and positions of multiple off-axis vortices loaded in the Gaussian beam. The focal-field characteristics of the hollow structured optical fields after passing through a lens are theoretically analyzed. On this basis, the experiments are implemented in the built optical system for multi-off-axis vortex beam focusing through an ordinary lens. In the experiments, various hollow structured optical fields are detected in CCD which are consistent with the theoretical results. The manipulations of size and rotation direction of the hollow structured optical fields are realized. We believe that this study will contribute to extending the potential applications of off-axis vortex beams in fields such as optical field shaping, optical manipulation and laser processing.

© 2023 Optica Publishing Group under the terms of the [Optica Open Access Publishing Agreement](#)

1. Introduction

The vortex beam [1,2] is a type of beam with a helical wavefront that contains a phase factor of $\exp(im\theta)$ in its complex amplitude (m is the topological charge and θ is the rotational azimuth). Due to the phase uncertainty in the central position of the helical wavefront, there is a phase singularity that causes the amplitude to vanish, so that the beam presents an annular intensity distribution. Vortex beams have important applications in optical field shaping [3], optical communication [4], optical trapping [5] and biomedicine [6]. Among them, using the properties of the phase singularity to generate novel optical fields with different spatial structures has become a research hotspot in the field of optical field manipulation.

With the development of manipulation of vortex beams, compared with the traditional single-vortex beams, the coaxial superposition of multiple vortices can generate new optical fields with richer phase distribution, intensity distribution and orbital angular momentum. In 2010, Guo et al. generated optical fields with triangular and pentagonal intensity distributions by coaxially superimposing two Laguerre-Gaussian beams with different mode indices and different relative amplitudes [7]. In 2014, Huang et al. superposed three coaxial Laguerre-Gaussian vortex beams with different topological charges and waist radius to generate a variety of three-ring structured optical fields [8]. Although the coaxial superposition of multiple vortices enriches the shaping

of optical field, due to multiple vortices are loaded on the optical axis center of the optical field and the multiple vortices coincide with each other, therefore the main way of optical field manipulation is to control the topological charge of each vortex. In this case, off-axis vortex beams which have an offset between the phase singularity of the vortex and the center of the host beam attracted the attention of researchers [9]. Compared with coaxial vortex beams, the number, off-axis distance and topological charge of vortices can all be used as the freedom degrees for optical field manipulation, which is expected to achieve more novel results of optical field shaping. In 2013, Anderson. M et al. obtained linear and angular shaped optical fields by modulating the arrangement of optical vortices [10]. In 2015, Kovalev et al. superposed the off-axis Bessel beams and obtained triangular and pentagonal structured optical fields by adjusting the weight coefficients and off-axis distances of multiple Bessel beams [11]. In 2016, Huang et al. generated optical fields with multiple optical dark-holes in the tightly focused field under a high numerical aperture objective lens by adding multiple off-axis vortices in a radial vector beam based on vector diffraction theory [12]. In 2017, Wang et al. achieved the generation of subwavelength equilateral polygon flat-top focal spots by superimposing off-axis vortex arrays in radially polarized beams based on the Richard-Wolf vector diffraction theory [13]. In 2019, Dong et al. realized the directional excitation of surface plasmon polaritons by using a radially polarized beam with multiple off-axis vortices based on the Richard-Wolf vector diffraction theory and Kretschmann-Raether three-layer structure theory [14]. Zhao et al. focused the radially polarized beam loaded with multiple off-axis vortices on a ZnSe crystal and generated second harmonics with non-circularly symmetric waveforms by changing the off-axis positions and number of multiple vortices [15]. In 2021, Wang et al. achieved the adjustment of the transmission trajectory and the intensity of the beam by setting the number and positions of off-axis vortices embedded in a circle Bessel-Gaussian vortex beam [16]. In summary, off-axis vortex beams have shown great potential and value in the fields such as optical field shaping and trajectory control of beams. Our group has generated a variety of regular polygonal flat-top focuses by arranging the positions of multiple off-axis vortices loaded in the radially polarized beam [13]. In this work, the focusing field is studied under the condition of tight focusing of a high numerical aperture objective lens in which the vector diffraction theory is adopted, and the size of the generated equilateral-polygon-like flat-top focus has the sub-wavelength level. It has important applications in the optical manipulation of irregularly shaped microparticles and hyperfine laser processing. However, for laser cutting, laser welding, surface treatment and other application scenarios that require a focus size of tens of microns and above, the tight focusing by a high numerical aperture objective lens ($NA > 0.7$) is no longer available. In this case, it is of practical significance to study the optical field shaping under ordinary lens focusing.

In this paper, we study the focal-field characteristics of the Gaussian beam loaded with multiple off-axis vortices after passing through an ordinary lens based on scalar diffraction theory and propose an optical field shaping method of off-axis vortex beam. Firstly, a variety of hollow structured optical fields are simulated by adjusting the number and positions of off-axis vortices. Then we study the propagation and focal-field characteristics of the hollow structured optical fields. In the experiments, we built an optical system of multi-off-axis vortex beams focused by an ordinary lens, in which the multiple off-axis vortices are loaded by a spatial light modulator (SLM) and the beam is focused by a convex lens with $f = 750$ mm ($NA = 0.017$). The hollow structured optical fields with a focus size of millimeter are detected by CCD. In addition, we achieved the manipulation of shape, size and rotation direction of the optical fields in the experiments. This work demonstrates the potential of off-axis vortex beams to generate complex structured optical fields and provides a new reference for the focusing shaping of off-axis vortex beams. The generated new structured optical fields have great potential in laser processing and optical manipulation.

2. Theoretical and numerical simulation

In cylindrical coordinates (ρ, θ, z) , when a beam propagates forward along the z -axis in free space, the complex amplitude of the optical field can be calculated theoretically through the Fresnel diffraction integral, which can be expressed as [17,18]:

$$E(\rho, \theta, z) = \frac{-ik}{2\pi z} \exp(ikz) \int_0^\infty \int_0^{2\pi} E_{in}(r, \varphi) \exp[i\frac{k}{2z}(r^2 + \rho^2)] \times \exp[i\frac{k}{z}\rho r \cos(\varphi - \theta)] r dr d\varphi \quad (1)$$

where $E_{in}(r, \varphi)$ is the initial optical field, r, φ are the radial distance and azimuth angle of the initial optical field. $E(\rho, \theta, z)$ is the distribution of the optical field at the axial distance z . ρ, θ are the radial distance and azimuth angle of the observation plane, k is the wave number.

In this paper, the multiple off-axis vortices are loaded into the Gaussian beam directly output from the laser. When an optical vortex with topological charge m_1 ($m_1 > 0$) is located at (r_1, φ_1) of the beam waist, the off-axis vortex beam can be expressed as:

$$E_{in}(r, \varphi) = E_0 \exp(-\frac{r^2}{w^2}) [r \exp(i\varphi) - r_1 \exp(i\varphi_1)]^{|m_1|} \quad (2)$$

where w is the waist radius of the incident Gaussian beam. Similarly, when the multiple off-axis vortices are loaded in the incident beam, the optical field of the beam can be expressed as [13,19]:

$$E_{in}(r, \varphi) = E_0 \exp(-\frac{r^2}{w^2}) \prod_{n=1}^N [r \exp(\pm i\varphi) - r_n \exp(\pm i\varphi_n)]^{|m_n|} \quad (3)$$

where $\prod_{n=1}^N [r \exp(\pm i\varphi) - r_n \exp(\pm i\varphi_n)]^{|m_n|}$ denotes the existence of n ($n = 1, 2, 3, \dots, N$) off-axis vortices in the beam, m_n is the topological charge of the n th off-axis vortex and (r_n, φ_n) is the position of the n th off-axis vortex. When $m_n > 0$, the sign of φ and φ_n are positive. When $m_n < 0$, the sign of φ and φ_n are negative.

According to Ref. [20], when vortices are loaded into the beam waist of a Gaussian beam, the size of the dark region of the optical field is controlled by the Gaussian waist radius w and the topological charge m of the vortex. In this paper, the width of the dark region corresponding to the reduction of the intensity of the optical field to $1/e$ of the maximum value is defined as the diameter d of the dark region of the optical field. Therefore, combined with Eq. (3), the number and positions of dark regions can be controlled by adjusting the number and positions of multiple off-axis vortices loaded in the Gaussian beam, so that the intensity of the optical field can be redistributed to obtain the desired optical field. For the convenience of discussion, we only consider the case that all topological charges are equal, that is, the topological charge $m_1 = m_2 = m_3 = \dots = m_n = +1$, in order to avoid the possibility of annihilation and repositioning of vortices [21].

In this paper, the distributions of off-axis vortices are designed with rotational symmetry. According to the number n of off-axis vortices, the vortices are distributed around the beam center with an equal radian interval $\Delta\varphi = \varphi_n - \varphi_{n-1} = 2\pi/n$ and the equal off-axis distance r . As shown in Fig. 1(a), the two off-axis vortices are distributed around the beam center with equal radian interval π and equal off-axis distance $r_1 = r_2 = 0.5$ mm (initial beam waist radius $w = 2$ mm). Similarly, the off-axis vortices in Figs. 1(b)-1(e) are equidistantly distributed around the beam center with equal radian intervals of $2\pi/3, \pi/2, 2\pi/5$, and $\pi/3$ respectively (the corresponding parameters in Fig. 1 are listed in Table 1). Since each vortex causes a helical phase with a 2π variation around the center of the vortex, the phase distributions show pinwheel shapes as shown in Figs. 1(f)-1(j). At this time, the intensity distributions of the optical fields in the x - y plane

and the three-dimensional graphs of normalized intensity of the corresponding optical fields are shown in Figs. 2(a)-2(e) and Figs. 2(f)-2(j), which show that the intensity distributions of optical fields present hollow structures. In Fig. 2(a), when two off-axis vortices are distributed around the beam center with π as equal radian interval and $r_1 = r_2 = 0.5$ mm as equal off-axis distance, the intensity distribution of the optical field presents a hollow elliptic structure. In Figs. 2(b)-2(e), when off-axis vortices with number $n = 3, 4, 5, 6$ are distributed around the beam center with equal radian intervals of $2\pi/3, \pi/2, 2\pi/5, \pi/3$ and equal off-axis distances of 0.8 mm, 1.1 mm, 1.4 mm, 1.5 mm, respectively, the corresponding intensity distributions of the optical fields present the hollow polygon structures including hollow triangle, hollow quadrangle, hollow pentagon and hollow hexagon. The number of sides of the polygons is equal to the number of loaded vortices.

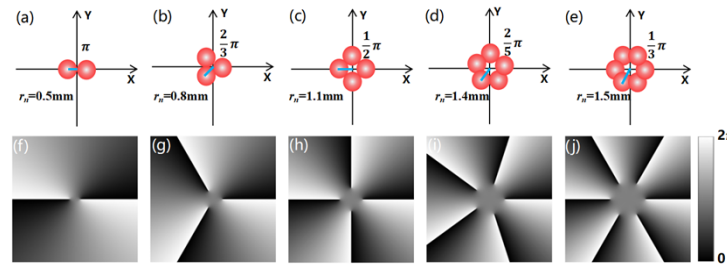


Fig. 1. (a)-(e) Positions of multiple off-axis vortices; (f)-(j) Phase distributions of the corresponding multiple off-axis vortices.

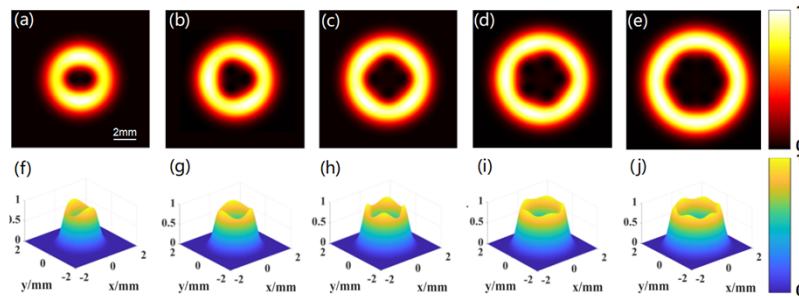


Fig. 2. (a)-(e) Theoretical simulations of intensity distributions of the hollow structured optical fields with the same parameters as Fig. 1 in the x-y plane; (f)-(j) Three-dimensional graphs of normalized intensity of the corresponding optical fields.

Table 1. Position parameters of the multiple off-axis vortices

number	Vortex number	radial distance(mm)	azimuth angle
(a)	$n = 2$	$r_1 = r_2 = 0.5$	$\varphi_1 = 0, \varphi_2 = \pi$
(b)	$n = 3$	$r_1 = r_2 = r_3 = 0.8$	$\varphi_1 = 0, \varphi_2 = 2\pi/3, \varphi_3 = 4\pi/3$
(c)	$n = 4$	$r_1 = r_2 = r_3 = r_4 = 1.1$	$\varphi_1 = 0, \varphi_2 = \pi/2, \varphi_3 = \pi, \varphi_4 = 3\pi/2$
(d)	$n = 5$	$r_1 = r_2 = r_3 = r_4 = r_5 = 1.4$	$\varphi_1 = 0, \varphi_2 = 2\pi/5, \varphi_3 = 4\pi/5, \varphi_4 = 6\pi/5, \varphi_5 = 8\pi/5$
(e)	$n = 6$	$r_1 = r_2 = r_3 = r_4 = r_5 = r_6 = 1.5$	$\varphi_1 = 0, \varphi_2 = \pi/3, \varphi_3 = 2\pi/3, \varphi_4 = \pi, \varphi_5 = 4\pi/3, \varphi_6 = 5\pi/3$

In order to generate more types of hollow structured optical fields, we increase off-axis distances of multiple vortices on the basis of Fig. 2. When the positions of off-axis vortices are set as shown in Figs. 3(a)-3(e), the corresponding phase distributions are shown in Figs. 3(f)-3(j),

respectively. At this time, the intensity distributions of the optical fields in the x-y plane and the three-dimensional graphs of normalized intensity of the corresponding optical fields are shown in Figs. 3(k)-3(o) and Figs. 3(p)-3(t) (the corresponding parameters in Fig. 3 are listed in Table 2). Compared with Fig. 2, the results in Fig. 3 indicate that as the off-axis distance increases, the dark regions gradually move out and separate from each other. It results that a stronger energy distribution appears in the center of the beams. The intensity distributions of the optical fields show various hollow button-shaped structures. The above research shows that the optical field intensity distributions can show various hollow structures by adjusting the number and positions of off-axis vortices. Besides, when the topological charge of each vortex is equal, the beam width expands with the increase of the vortex number.

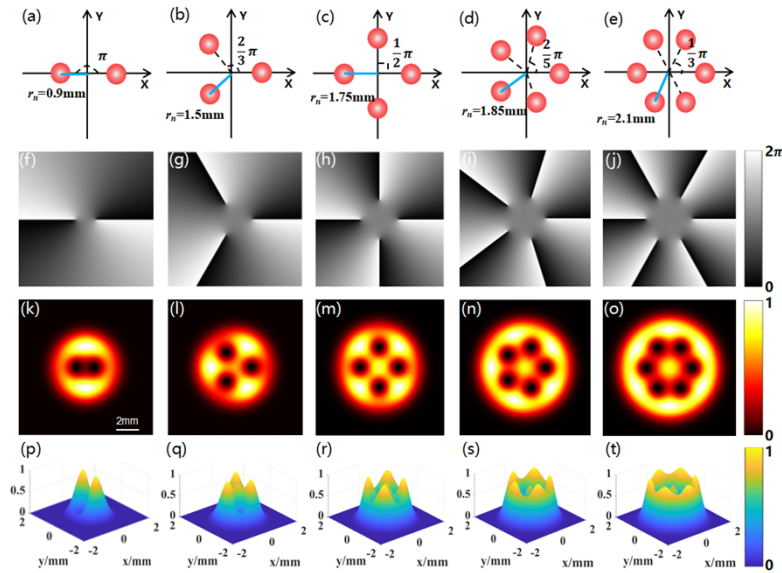


Fig. 3. (a)-(e) Positions of multiple off-axis vortices of the hollow button-shaped structured optical fields; (f)-(j) Phase distributions of the corresponding off-axis vortices; (k)-(o) Theoretical simulations of intensity distributions of the hollow button-shaped structured optical fields in the x-y plane; (p)-(t) Three-dimensional graphs of normalized intensity of the corresponding optical fields.

Table 2. Position parameters of multiple off-axis vortices of the hollow button-shaped structured optical fields

number	Vortex number	radial distance(mm)	azimuth angle
(a)	$n = 2$	$r_1 = r_2 = 0.9$	$\varphi_1 = 0, \varphi_2 = \pi$
(b)	$n = 3$	$r_1 = r_2 = r_3 = 1.5$	$\varphi_1 = 0, \varphi_2 = 2\pi/3, \varphi_3 = 4\pi/3$
(c)	$n = 4$	$r_1 = r_2 = r_3 = r_4 = 1.75$	$\varphi_1 = 0, \varphi_2 = \pi/2, \varphi_3 = \pi, \varphi_4 = 3\pi/2$
(d)	$n = 5$	$r_1 = r_2 = r_3 = r_4 = r_5 = 1.85$	$\varphi_1 = 0, \varphi_2 = 2\pi/5, \varphi_3 = 4\pi/5, \varphi_4 = 6\pi/5, \varphi_5 = 8\pi/5$
(e)	$n = 6$	$r_1 = r_2 = r_3 = r_4 = r_5 = r_6 = 2.1$	$\varphi_1 = 0, \varphi_2 = \pi/3, \varphi_3 = 2\pi/3, \varphi_4 = \pi, \varphi_5 = 4\pi/3, \varphi_6 = 5\pi/3$

The above research shows the intensity distributions of various hollow structured optical fields generated by manipulating off-axis vortices in the x-y plane. In order to study the propagation characteristics of the hollow structured optical fields, we use the matrix multiplication arithmetic [22] to numerically simulate the propagation of the hollow structured optical fields shown in Fig. 2 in free space, and the results are shown in Fig. 4 (the incident beam $w = 2$ mm, $\lambda = 632.8$ nm).

As seen from Fig. 4, in free space, the beams can maintain stable transmission along the optical axis and maintain the optical field structures over a long range of propagation. With the increase of propagation distance, the optical fields rotate transversely around the propagation axis (when $m > 0$, the optical field rotates anticlockwise) and beam widths expand. During the propagation distance z from 0 to infinity, the overall rotation of the optical fields is 90° , which is introduced by the Gouy phase shift of the vortex beam [9,23,24]. The rotation angle can be calculated by $\theta(z) = \arctan(z/z_R)$, where $z = 0$ is the beam waist position, and z_R is Rayleigh distance, when $w = 2$ mm and $\lambda = 632.8$ nm, $z_R = \pi w^2 / \lambda = 19848$ mm.

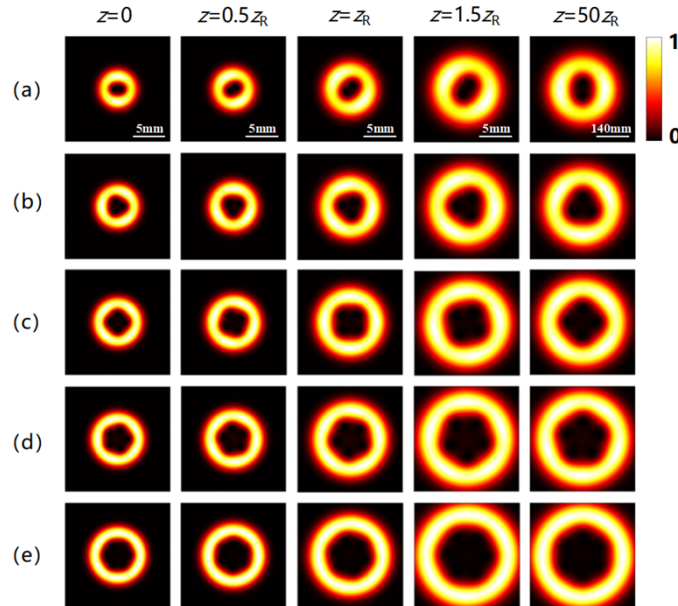


Fig. 4. Theoretical simulations of intensity distributions of the hollow structured optical fields with the same parameters as Fig. 2 at different propagation distances z in free space. The number of loaded vortices is (a) $n = 2$, (b) $n = 3$, (c) $n = 4$, (d) $n = 5$, (e) $n = 6$, respectively. The scale of each column of optical fields is the same.

Based on the above research, in order to further study the focal-field characteristics of the hollow structured optical fields, we add an ordinary lens in the optical path. We choose a convex lens with a focal length $f = 750$ mm ($NA = 0.017$) to focus the beams. For the hollow structured optical fields with the same parameters as Fig. 2, the simulation results are shown in Fig. 5. We set the focal position as $z = 0$ mm, where $z < 0$ in front of the focus and $z > 0$ behind the focus. For the hollow elliptical optical field, we quantitatively analyze the size change of the optical fields during the focusing by calculating the change of the semi-major axis t (the distance between the center of the dark region and the point on the semi-major axis where the intensity of the optical field decreases to $1/e$ of the maximum value) of the central elliptical dark region. And for the hollow structured optical fields whose dark regions are ellipse, triangle, quadrilateral, pentagon and hexagon, we quantitatively analyze the size change of the optical fields during the focusing by calculating the distance l between the center of the polygonal dark region and a vertex, that is, the farthest distance between the center of the polygonal dark region and the point on the angular bisector where the intensity of the optical field decreases to $1/e$ of the maximum value. In addition, we define the focal spot diameter corresponding to the intensity of the optical field at the focus decreases to $1/e$ of the maximum value as the focal size. In Fig. 5, we can see that the rotation direction of the structured optical fields within $z < 0$ is opposite to that within

the $z > 0$ due to the Gouy phase shift (clockwise rotation when $z < 0$ and anticlockwise rotation when $z > 0$) except for the size change of the structured optical field in front of and behind the focus. In the range of $z = \pm 80$ mm, the parameter l of the elliptical dark region of hollow elliptical optical field changes from 0.05 mm to 0.15 mm. The parameter l of the triangular dark region of hollow triangular optical field changes from 0.06 mm to 0.19 mm. The parameter l of the quadrilateral dark region of hollow quadrilateral optical field changes from 0.07 mm to 0.21 mm. The parameter l of the pentagonal dark region of hollow pentagonal optical field changes from 0.08 mm to 0.26 mm, and the parameter l of the hexagonal dark region of hollow hexagonal optical field changes from 0.09 mm to 0.29 mm. At the focus, the focal sizes of the hollow elliptical optical field, the hollow triangular optical field, the hollow quadrilateral optical field, the hollow pentagonal optical field and the hollow hexagonal optical field are 0.20 mm, 0.21 mm, 0.23 mm, 0.26 mm and 0.28 mm, respectively.

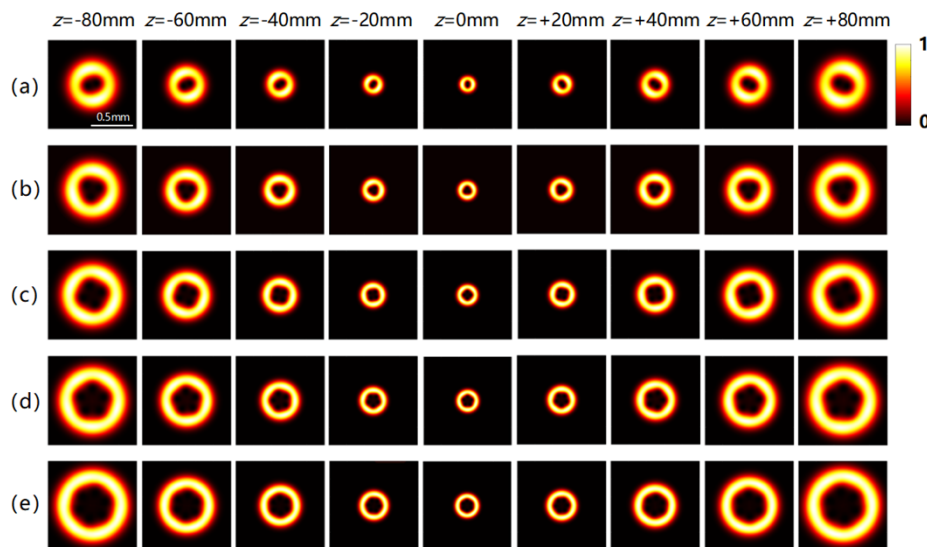


Fig. 5. Theoretical simulations of focal-field intensity distributions of the hollow structured optical fields with the same parameters as Fig. 2 at different distances z .

The simulation results of focal-field intensity distributions of the hollow button-shaped structured optical fields with the same parameters as Fig. 3 are shown in Fig. 6. For the hollow button-shaped structured optical fields, since the dark regions in the optical fields are separated from each other, we quantitatively analyze the size change of the optical field by calculating the change of the diameter d of one dark region during the focusing. In Fig. 6, the hollow button-shaped optical fields also rotate anticlockwise when $z > 0$, and the optical fields rotate clockwise when $z < 0$. In the range of $z = \pm 80$ mm, the diameter d of one dark region ranges from 0.05 mm to 0.16 mm. At the focus, the focal sizes of the hollow button-shaped structured optical fields with two holes, three holes, four holes, five holes and six holes are about 0.25 mm, 0.30 mm, 0.33 mm, 0.36 mm and 0.39 mm, respectively. According to the Gaussian beam focusing formula $d = 4M^2 \lambda f / \pi D$ (d is the diameter of the focus, λ is the beam wavelength, M^2 is the beam quality factor of the laser and D is the beam diameter through the lens), when the laser parameters of the experimental system and the beam diameter D are constant, the size of the focus is proportional to the lens focal length. Therefore, the manipulation of the focus size can be achieved by changing the lens focal length. The above research results show that a variety of hollow structured optical fields can be generated by adjusting the number and positions of multiple off-axis vortices in the host beam, and the size and rotation direction of hollow structured

optical fields can be adjusted by selecting the appropriate optical system (considering the focal length of the lens and the position of the lens).

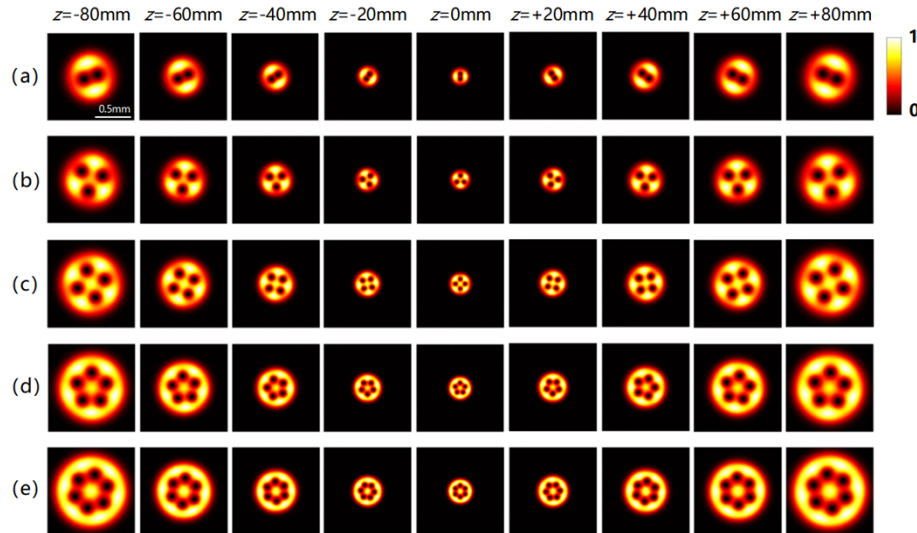


Fig. 6. Theoretical simulations of focal-field intensity distributions of the hollow button-shaped structured optical fields with the same parameters as Fig. 3 at different distances z .

3. Experimental results

To verify the effectiveness of the above theoretical simulations, we built an optical system for multi-off-axis vortex beams focusing and detecting, as shown in Fig. 7. The central wavelength of laser is 632.8 nm (He-Ne laser with type of 25-LHP-151-230, linearly polarized laser output). The Gaussian beam output from the laser is expanded by the beam expanding system. The polarization direction and polarization purity of the beam are adjusted by the half wave plate (HWP) and the polarizer. Later, the beam is incident on the reflective spatial light modulator (HOLOEYE, HES-6010-0467, pixel size $8\ \mu\text{m} \times 8\ \mu\text{m}$, resolution 1920×1080 pixels) loading multi-off-axis vortex phase diagram. After the beam is modulated and reflected by the SLM, it is focused by a convex lens. To make full use of the pixels of CCD and reduce the experimental error of optical field detection, we choose a convex lens (L2) with a focal length $f = 750$ mm to focus the beam. When the beam is focused by L2, the optical field intensity distributions at different distances z are recorded by a CCD (DH-130UM, pixel size $5.2\ \mu\text{m} \times 5.2\ \mu\text{m}$, pixel number 1280×1024) mounted on a sliding track.

When there is no lens L2, and the multi-off-axis vortex phase diagrams of Figs. 1(f)-1(j) and Figs. 3(f)-3(j) are loaded onto SLM respectively, the optical field intensity distributions recorded by the CCD are shown in Figs. 8(a)-8(e) and Figs. 8(f)-8(j), respectively. It can be seen from Figs. 8(a)-8(e) that the optical field intensity distributions present hollow structures and the dark regions are ellipse, triangle, quadrilateral, pentagon and hexagon, respectively. In Figs. 8(f)-8(j), as the off-axis distance of off-axis vortices increases, the dark regions gradually move out and separate from each other. The optical field intensity distribution shows a hollow button-shaped structure with two holes, three holes, four holes, five holes and six holes, respectively. Therefore, in addition to the error of optical field intensity change caused by laser beam expansion, and some diffraction effects and distortion lines caused by optical element aperture and SLM modulation

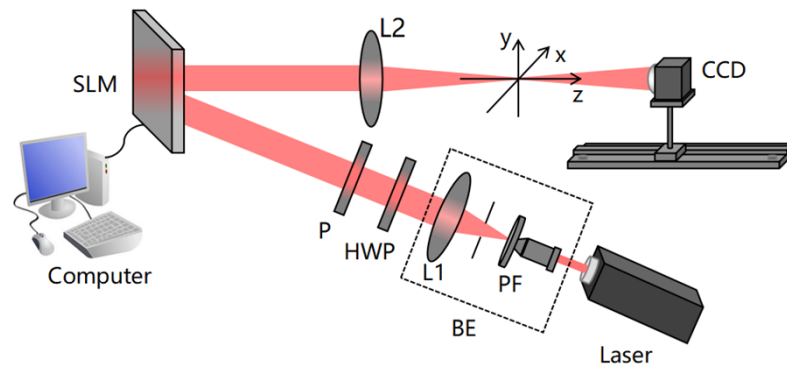


Fig. 7. The schematic of the optical experimental system. BE: Beam expander, PF: Pinhole filter, L1: Lens ($f=100$ mm), HWP: Half wave plate, P: Polarizer, SLM: Spatial light modulator, L2: Lens ($f=750$ mm), CCD: Charge coupled device.

respectively, the experimental results of the dark region shape of optical fields are consistent with the simulated results in Figs. 2(a)-2(e) and Figs. 3(k)-3(o).

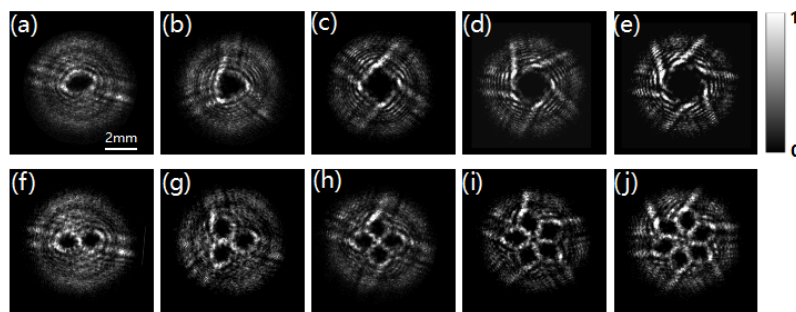


Fig. 8. (a)-(e) Recorded graphs of intensity distributions of the hollow structured optical fields with the same parameters as Fig. 2; (f)-(j) Recorded graphs of intensity distributions of hollow button-shaped structured optical fields with the same parameters as Fig. 3.

In order to analyze the focal-field characteristics of the hollow structured optical fields, the phase diagrams of Figs. 1(f)-1(j) are loaded onto SLM respectively, and then the modulated beams are focused by the convex lens L2. The intensity distributions of optical fields at different distances z recorded by the CCD are shown in Fig. 9. As shown in Fig. 9, the size of the hollow structured optical fields changes and the optical fields rotate around the propagation axis as the distance $|z|$ increases. The optical fields rotate anticlockwise when $z > 0$, and the optical fields rotate clockwise when $z < 0$, which are consistent with the theoretical simulation results. In this experiment, in the range of $z = \pm 80$ mm, the parameter t of the elliptical dark region of hollow elliptical optical field changes from 0.06 mm to 0.16 mm. The parameter l of the triangular dark region of hollow triangular optical field changes from 0.07 mm to 0.21 mm. The parameter l of the quadrilateral dark region of hollow quadrilateral optical field changes from 0.08 mm to 0.24 mm. The parameter l of the pentagonal dark region of hollow pentagonal optical field changes from 0.09 mm to 0.25 mm, and the parameter l of the hexagonal dark region of hollow hexagonal optical field changes from 0.11 mm to 0.28 mm. In order to more intuitively observe the consistency between the experimental results and simulation results, the simulation and experimental measurement results of the parameters t and l at different distances z are shown in Fig. 10. It can be seen from Figs. 10 that the experimental results of the dark region size

change of the hollow structured optical fields are consistent with the simulation results. In addition, at the focus, the focal sizes of the hollow elliptical optical field, the hollow triangular optical field, the hollow quadrilateral optical field, the hollow pentagonal optical field and the hollow hexagonal optical field are about 0.23 mm, 0.24 mm, 0.27 mm, 0.29 mm and 0.32 mm, respectively. Through numerical comparisons, the experimental results are basically consistent with the simulation results.

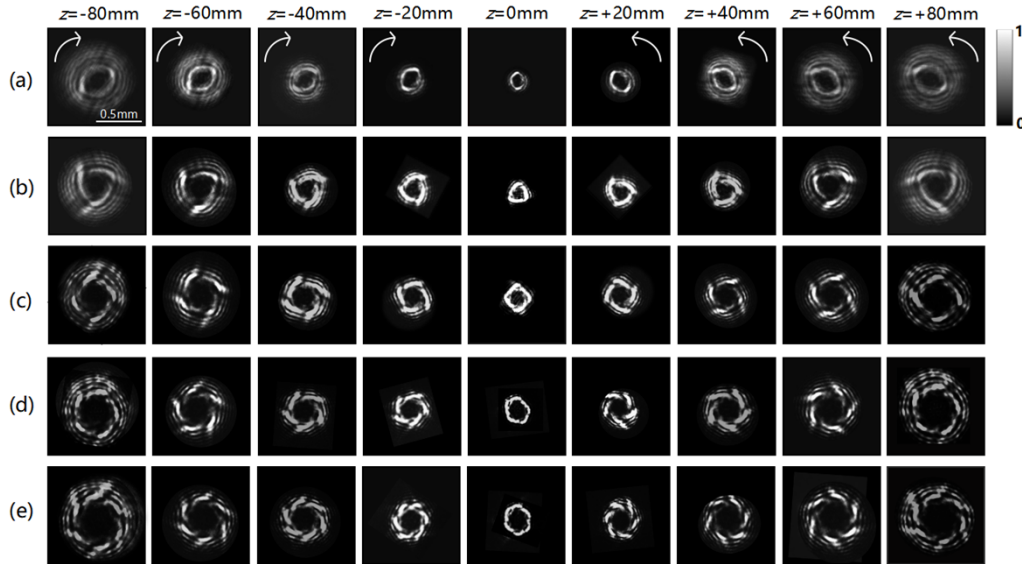


Fig. 9. Recorded graphs of focal-field intensity distributions of the hollow structured optical fields with the same parameters as Fig. 2 at different distances z . The number of loaded vortices is (a) $n = 2$, (b) $n = 3$, (c) $n = 4$, (d) $n = 5$, (e) $n = 6$, respectively.

Similarly, to further analyze the focal-field characteristics of the hollow button-shaped structured optical fields, the phase diagrams of Figs. 3(f)-3(j) are loaded onto SLM respectively, and the modulated beams are focused by the convex lens L2. The focusing intensity distributions of optical fields recorded by CCD are shown in Fig. 11. As shown in Fig. 11, the optical fields rotate anticlockwise when $z > 0$ and the optical fields rotate clockwise when $z < 0$. In this experiment, in the range of $z = \pm 80$ mm, the diameter d of one dark region varies from 0.06 mm to 0.17 mm. Similarly, in order to more intuitively observe the consistency between the experimental results and simulation results. The simulation and experimental measurement results of the parameters d at different distances z are shown in Fig. 12. It can be seen from Figs. 12 that the experimental results of the size change of one dark region of the hollow button-shaped structured optical fields are consistent with the simulation results. At the focus, the focal sizes of the hollow button-shaped structured optical fields with two holes, three holes, four holes, five holes and six holes are about 0.27 mm, 0.33 mm, 0.35 mm, 0.39 mm and 0.42 mm, respectively. Through numerical comparisons, the experimental results are also basically consistent with the simulation results.

The above results show that the manipulation of the shape, size and rotation direction of the hollow structured optical field can be realized by designing multi-off-axis vortex beam parameters and combining with the focusing lens. Compared with other optical field shaping methods [11,25] that generate similar shapes, the optical field shaping method in this paper can directly control the number and position of off-axis vortices loaded in a Gaussian beam to generate a variety of hollow structured optical fields, and can easily control the characteristic size of the optical fields

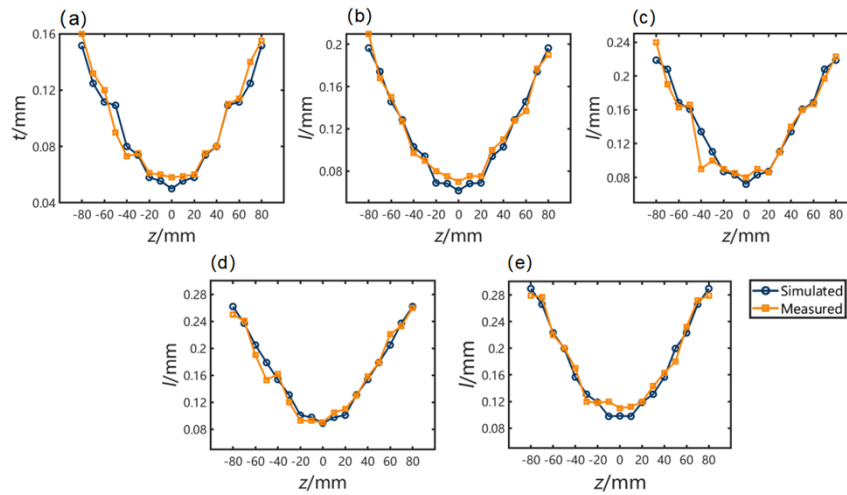


Fig. 10. Simulated and experimental measured results of dark region parameters of the hollow structured optical fields with the same parameters as Fig. 2 at different distances z . (a) t of the hollow elliptical optical field; (b) l of the hollow triangular optical field; (c) l of the hollow quadrilateral optical field; (d) l of the hollow pentagonal optical field; (e) l of the hollow hexagonal optical field.

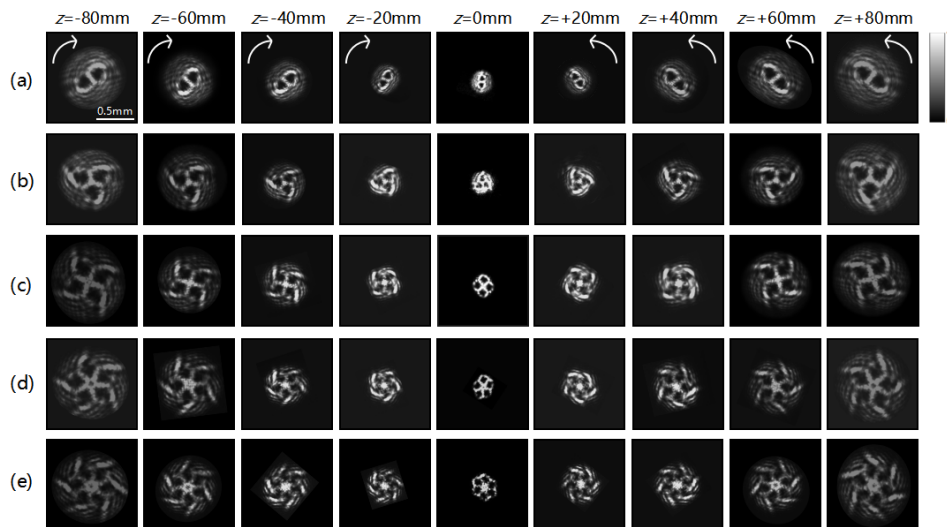


Fig. 11. Recorded graphs of focal-field intensity distributions of the hollow button-shaped structured optical fields with the same parameters as Fig. 3 at different distances z . The number of loaded vortices is (a) $n = 2$, (b) $n = 3$, (c) $n = 4$, (d) $n = 5$, (e) $n = 6$, respectively.

by changing the focusing ability of the lens to make it tens of microns and above. Therefore, the optical field shaping method in this paper is simpler and more flexible, and the types of generated structured optical fields are more abundant, which have great potential in larger size pattern laser processing [26,27] and the fabrication of optical lattices [28]. In addition, compared with the Gerchberg-Saxton (GS) algorithm [29] which is generally approved for generating the desired optical field, our method does not require repeated iterative calculations and is easier to achieve and more accurate in the processing of phase plate thanks to the continuous distribution

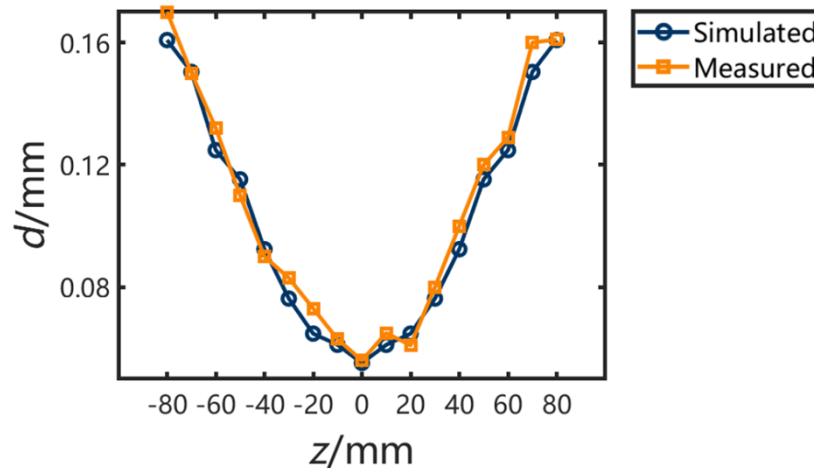


Fig. 12. Simulated and experimental measured results of parameter d of one dark region of the hollow button-shaped structured optical fields with the same parameters as Fig. 3 at different distances z .

of the vortex phase. Moreover, since the characteristic size of the hollow structured optical fields generated in our work matches the terahertz wavelength (30 μm -3 mm), these structured optical fields have outstanding application potential in the preparation of functional devices in the terahertz band [30–32].

4. Conclusion

Based on the scalar diffraction theory, optical field distributions of multi-off-axis vortex beams and their focusing field characteristics through an ordinary lens are studied in this paper. Various hollow structured optical fields including hollow ellipse, hollow triangle, hollow quadrangle, hollow pentagon, hollow hexagon and hollow button-shaped are obtained in simulations and experiments by adjusting the number and positions of multiple off-axis vortices loaded in a Gaussian beam. Moreover, the focal size and rotation direction of generated hollow structured optical fields can be manipulated by a convex lens focusing. The research results enrich the shaping methods of vortex beams and show great potential in laser etching of precision parts [33], laser processing with controllable shape, capture and manipulation of large size particles [34] and other fields.

Funding. National Natural Science Foundation of China (61875093, 12174196, 11904073); State Key Laboratory of Intense Pulsed Radiation Simulation and Effect (SKLIPR2123); State Key Laboratory of Applied Optics (SKLAO2022001A17).

Disclosures. The authors declare that there are no conflicts of interest related to this article.

Data availability. Data underlying the results presented in this paper are not publicly available at this time but may be obtained from the authors upon reasonable request.

References

1. P. Ju, W. Fan, W. Gao, Z. Li, Q. Gao, G. Li, X. Jiang, and T. Zhang, "Generation of perfect vectorial vortex beams by employing coherent beam combining," *Opt. Express* **31**(7), 11885–11898 (2023).
2. Y. Shen, X. Wang, Z. Xie, C. Min, X. Fu, Q. Liu, M. Gong, and X. Yuan, "Optical vortices 30 years on: OAM manipulation from topological charge to multiple singularities," *Light: Sci. Appl.* **8**(1), 90 (2019).
3. C. Guo, Y. Zhang, Y. Han, J. Ding, and H. Wang, "Generation of optical vortices with arbitrary shape and array via helical phase spatial filtering," *Opt. Commun.* **259**(2), 449–454 (2006).
4. H. Zhou, J. Dong, L. Shi, D. Huang, and X. Zhang, "Hybrid coding method of multiple orbital angular momentum states based on the inherent orthogonality," *Opt. Lett.* **39**(4), 731–734 (2014).

5. D. G. Grier, "A revolution in optical manipulation," *Nature* **424**(6950), 810–816 (2003).
6. S. Segawa, Y. Kozawa, and S. Sato, "Resolution enhancement of confocal microscopy by subtraction method with vector beams," *Opt. Lett.* **39**(11), 3118–3121 (2014).
7. Q. Guo and D. Deng, "Dynamics of collinear Laguerre-Gaussian beams in nonlocal nonlinear media," *Appl. Phys. B* **100**(4), 897–902 (2010).
8. S. Huang, T. Gu, Z. Miao, C. He, and T. Wang, "Experimental study on multiple-ring vortex beams," *Acta Phys. Sin.* **63**(24), 244103 (2014).
9. G. Liang and A. Wang, "Trajectories and rotations controlled off-axis winding beams in nonlocal nonlinear media," *Opt. Express* **27**(15), 21185–21193 (2019).
10. M. A. Anderson, E. L. Falco-Filho, and C. B. D. Araújo, "Shaping optical beams with topological charge," *Opt. Lett.* **38**(9), 1579–1581 (2013).
11. A. A. Kovalev and V. V. Kotlyar, "Orbital angular momentum of superposition of identical shifted vortex beams," *J. Opt. Soc. Am. A* **32**(10), 1805–1810 (2015).
12. S. Huang, X. Wang, Z. Zhu, L. Gong, B. Zhu, and L. Song, "Focusing field of the radial vector beams with multi-vortex phases," *Opt. Commun.* **366**, 142–147 (2016).
13. X. Wang, B. Zhu, Y. Dong, S. Wang, Z. Zhu, F. Bo, and X. Li, "Generation of equilateral-polygon-like flat-top focus by tightly focusing radially polarized beams superposed with off-axis vortex arrays," *Opt. Express* **25**(22), 26844–26852 (2017).
14. Y. Dong, S. Xi, B. Zhu, X. Wang, Q. Mu, S. Wang, and Z. Zhu, "The directional excitation of surface plasmon polaritons by radially polarized beam with multiple off-axis vortices," *Opt. Commun.* **443**, 197–201 (2019).
15. J. Zhao, B. Zhu, S. Xi, Q. Mu, S. Wang, Y. Dong, X. Wang, and Z. Zhu, "Second-harmonic wave patterns induced by the tightly focused radially polarized beam loaded with off-axis vortices," *Appl. Phys. B: Lasers Opt.* **125**(8), 139 (2019).
16. H. Wang, C. Sun, J. Tu, W. Zhen, and D. Deng, "Propagation dynamics and radiation forces of autofocusing circle Bessel Gaussian vortex beams in a harmonic potential," *Opt. Express* **29**(18), 28110–28123 (2021).
17. C. Paterson and R. Smith, "Higher-order Bessel waves produced by axicon-type computer-generated holograms," *Opt. Commun.* **124**(1-2), 121–130 (1996).
18. Y. Geng, W. Huang, J. Yang, Y. Qian, Z. Ren, and P. Yu, "Generation of Mathieu beams based on the detour phase encoding method," *Opt. Commun.* **486**, 126754 (2021).
19. G. Indebetouw, "Optical Vortices and Their Propagation," *J. Mod. Opt.* **40**(1), 73–87 (1993).
20. G. Zhou, Y. Cai, and C. Dai, "Hollow vortex Gaussian beams," *Sci. China Phys. Mech. Astron.* **56**(5), 896–903 (2013).
21. J. Leach, M. R. Dennis, J. Courtial, and M. J. Padgett, "Vortex knots in light," *New J. Phys.* **7**, 55 (2005).
22. H. Gong, G. Li, Q. Chen, L. Fang, and C. Zhou, "Study of an arithmetic for fast computing transmission of light field," *Acta Opt. Sin.* **36**(4), 405001 (2016).
23. S. M. Baumann, D. M. Kalb, L. H. Macmillan, and E. J. Galvez, "Propagation dynamics of optical vortices due to Gouy phase," *Opt. Express* **17**(12), 9818–9827 (2009).
24. Y. Ming, Y. Intaravanne, H. Ahmed, M. Kenney, Y. Lu, and X. Chen, "Creating Composite Vortex Beams with a Single Geometric Metasurface," *Adv. Mater.* **34**(18), 2109714 (2022).
25. S. Huang, Z. Miao, C. He, F. Pang, Y. Li, and T. Wang, "Composite vortex beams by coaxial superposition of Laguerre-Gaussian beams," *Opt Lasers Eng* **78**, 132–139 (2016).
26. M. Zukerstein, J. Hrabovsky, J. Sladek, I. Mirza, Y. Levy, and N. M. Bulgakova, "Formation of tubular structures and microneedles on silicon surface by doughnut-shaped ultrashort laser pulses," *Appl. Surf. Sci.* **592**, 153228 (2022).
27. L. Yang, D. Qian, C. Xin, Z. Hu, S. Ji, D. Wu, Y. Hu, J. Li, W. Huang, and J. Chu, "Direct laser writing of complex microtubes using femtosecond vortex beams," *Appl. Phys. Lett.* **110**(22), 221103 (2017).
28. X. Wang, Z. Zhang, Y. Gao, S. Zhao, Y. Jie, and C. Zhao, "Investigation on the Formation of Laser Transverse Pattern Possessing Optical Lattices," *Front. Phys.* **9**, 2296–4242 (2022).
29. H. Pang, W. Liu, A. Cao, and Q. Deng, "Speckle-reduced holographic beam shaping with modified Gerchberg-Saxton algorithm," *Opt. Commun.* **433**, 44–51 (2019).
30. B. Feng, E. Liu, Z. Wang, W. Cai, H. Liu, S. Wang, T. Liang, W. Xiao, and J. Liu, "Generation of terahertz hollow beams by a photonic quasi-crystal flat lens," *Appl. Phys. Express* **9**(6), 062003 (2016).
31. S. F. Busch, M. Weidenbach, J. C. Balzer, and K. Martin, "THz Optics 3D Printed with TOPAS," *J. Infrared, Millimeter, Terahertz Waves* **37**(4), 303–307 (2016).
32. H. Xin and M. Liang, "3-D-Printed Microwave and THz Devices Using Polymer Jetting Techniques," *Proc. IEEE* **105**(4), 737–755 (2017).
33. J. K. Gansel, M. Thiel, M. S. Rill, M. Decker, K. Bade, V. Saile, G. von Freymann, S. Linden, and M. Wegener, "Gold helix photonic metamaterial as broadband circular polarizer," *Science* **325**(5947), 1513–1515 (2009).
34. J. Wen, B. Gao, G. Zhu, D. Liu, and L. Wang, "Precise position and angular control of optical trapping and manipulation via a single vortex-pair beam," *Opt Lasers Eng* **148**, 106773 (2022).